N-doped microporous carbon microspheres for high volumetric performance supercapacitors

G.A. Ferrero, A. B. Fuertes, M. Sevilla*

Instituto Nacional del Carbón (CSIC), P.O. Box 73, Oviedo 33080, Spain

* Corresponding author: martasev@incar.csic.es

Abstract

N-doped highly dense uniform carbon microspheres of around 1 μm have been prepared by a nanocasting strategy using silica particles as template and a nitrogen-rich substance (*i.e.* pyrrole) as carbon precursor. These carbon microspheres possess a large number of nitrogen functional groups (~ 9 wt % N), a high BET surface area of up to ~ 1300 m^2 g^{-1} with a porosity made up mostly of micropores (< 2 nm), and a high packing density of 0.97 g cm^{-3}. They also show a remarkable volumetric capacitance of *ca*. 290 F cm^{-3} in H_2SO_4 as a result of pseudocapacitance effects arising from the N-groups, such that they are able to keep 50 % of the capacitance at a high current density of 40 A g^{-1}. An additional chemical activation process with KOH has been performed to enhance the microporous network. These highly porous microspheres (2690 m^2 g^{-1}), that have a lower nitrogen content (~ 2 % wt), can achieve 92 F cm^{-3} in $TEABF_4$/AN while displaying 83 % of capacitance retention at a high current density of 40 A g^{-1}.

Keywords: carbon, volumetric, supercapacitors, sphere, nitrogen-doping.

1. Introduction

Electrical double layer capacitors (EDLCs), also called supercapacitors or ultracapacitors, are considered to be a promising high power energy source for portable electronic devices, cold-starting assistants, electric vehicles and so on, as a result of their better rate capability and longer cyclic life compared to secondary batteries [1-3]. High surface area carbon materials have been recognized as the most promising, user-friendly electrode materials due to their low cost, wide availability, non-toxic nature, environmental friendliness, and stability [2-7].

Carbon materials usually store charges in an electrical double-layer formed at the interface between the electrode and the electrolyte. Therefore, their capacitance depends mostly on the surface area accessible to the electrolyte, and the main factors influencing their electrochemical performance being their specific surface area and pore-size distribution [3, 5, 7]. In general, carbon materials with high specific surface areas and a large number of narrow micropores have a higher capability for charge accumulation at the electrode/electrolyte interface [6, 7]. In addition, capacitance performance can be improved by the incorporation of certain types of heteroatoms such as nitrogen into the carbon framework [3, 8]. Indeed, it has been reported that N-doped porous carbons clearly exhibit a superior performance as supercapacitors due to an enhancement of their electronic conductivity and surface wettability in addition to the pseudo-capacitive effects contributed by the nitrogen functional groups [6, 9-11].

Enhancement of the gravimetric energy and power densities has traditionally been the main objective in relation to the use of porous carbon materials as supercapacitors. By contrast, optimization of the performance of the carbon supercapacitor in terms of volumetric properties (*i.e.* capacitance, and stored energy and power) has normally been ignored in the scientific literature. Yet, this is an important issue that recently has generated a great deal of attention from the application standpoint due to the recent development of portable, compact energy storage systems [12-14]. The porous carbons used in supercapacitors are normally made up of particles with an irregular morphology and a high porosity which give rise to low packing densities, usually < 0.6 g cm^{-3} [12]. This negative characteristic implies that, in spite of their high specific gravimetric capacitances and energy densities, many of these materials suffer a significant reduction in volumetric performance that makes them less competitive for the above-mentioned applications. Therefore, the fabrication of porous carbon materials with a high gravimetric and volumetric performance is still an important challenge to be overcome [15]. In recent literature, several attempts to fabricate materials with a high volumetric energy density can be found, most of them based on the use of carbon nanotubes or graphene materials as substrates [16-20].

In order to achieve a high volumetric energy density it is important to optimize the porosity and minimize the volume of the interparticle voids in order to increase the packing density of the carbon electrodes. A common way to attain this objective is to fabricate densified carbon monoliths. This approach has been successfully tested with carbide-derived carbons (CDCs) [21], and graphene materials [22, 23]. An alternative strategy is to use carbon particles

with an appropriate morphology in order to maximize the packing density. In particular, uniform porous carbon microspheres are a good option seeing that the assembly of such particles with a spherical morphology can attain a large packing density of up to 74 % of the sphere density, a value much higher than that achieved with irregular-shaped particles [24-26]. In this case, it can be expected that the interparticle voids between the microspheres will act as buffer reservoirs ensuring a good electrolyte accessibility despite the dense packing [27-30].

In the present work, we report a synthesis strategy for the fabrication of N-doped porous carbon microspheres with a diameter of around 1 μm. These carbon particles possess several important properties that make them highly useful in EDLC systems: i) a large number of nitrogen functional groups that provide enhanced capacitive properties, ii) a spherical morphology that guarantees a high packing density of up to 0.97 g cm^{-3}, and iii) a large BET surface area of up to ~ 2700 m^2 g^{-1} and a porosity consisting principally of micropores (< 2 nm). The carbon microspheres were synthesized by means of a nanocasting technique based on the use of porous silica particles as template. Significantly, a nitrogen-rich substance (pyrrole) was used as carbon precursor, yielding a carbon material with a large number of nitrogen groups. An additional chemical activation step with KOH was used to increase the microporous network.

2. Experimental section

2.1 Preparation of the porous N-doped carbon microspheres

The N-doped carbon particles were produced by means of a nanocasting strategy based on the use of porous silica microspheres as template and pyrrole (Aldrich, 99%) as N-containing carbon precursor. The template was synthesized as reported in detail elsewhere [31] and the infiltration of the carbon precursor was carried out by vapor impregnation. To this end, a 2 M solution of $FeCl_3$ in ethanol was added drop-wise to the silica particles in order to obtain 0.30 g $FeCl_3$/g silica. Then, the $FeCl_3$-impregnated silica sample was exposed, in a closed vessel, to pyrrole vapors at 25 ºC for 22 h. The dark solid thus obtained was heat-treated under N_2 up to the desired carbonization temperature (*i.e*. 600, 700 or 850 ºC) at a rate of 3 ºC min^{-1} for 1 h. Finally, the carbonized composite was treated with hydrofluoric acid (48%) to dissolve the silica framework. The resulting carbon residue was collected by filtration, washed with distilled water, and dried at 120 ºC for several hours. The resulting N-doped carbon microspheres are denoted as *N-CS-X*, where *X* represents the carbonization temperature in ºC.

In order to increase the specific surface area and the micropore volume, the templated carbon spheres were chemically activated with KOH, as reported in detail elsewhere [32]. Briefly, a 6 M aqueous solution of KOH was added drop-wise to the carbon sample in order to achieve a KOH/carbon weight ratio of 1. The impregnated sample was dried under vacuum at 50 ºC for several hours and then, it was heat-treated at 800 ºC (3 ºC min^{-1}) for 1 h under N_2. Finally, the solid residue was washed three times with HCl (10%) to remove the potassium compounds and then with distilled water, after which the carbon particles were collected by centrifugation and dried at 120 ºC for several hours. This type of

carbon spheres was designated as *N-CSA-X*, where *X* represents the carbonization temperature in ºC.

2.2 Materials Characterization

The morphology of the powders was examined by scanning (SEM, Zeiss DSM 942) and transmission (TEM, JEOL-2000 FXII) electron microscopy. The particle size distribution was obtained from several SEM pictures by measuring 100-150 particles. Nitrogen sorption and isotherms were recorded at -196 ºC using a Micromeritics ASAP 2020 volumetric physisorption system. The Brunauer-Emmett-Teller (BET) surface area was deduced from an analysis of the isotherm in the relative pressure range of 0.04-0.20. The total pore volume was calculated from the amount of nitrogen adsorbed at a relative pressure of 0.90. The micropore volume (V_{mi}), the micropore surface area (S_{mi}) and the pore size distributions were determined by applying the quenched-solid density functional theory (QSDFT) method to the nitrogen adsorption data and assuming a slit pore model. X-ray photoelectron spectroscopy (XPS) was performed on a Specs spectrometer, using Mg Kα (1253.6 eV) radiation delivered by a double anode at 150 W. X-ray diffraction (XRD) patterns were obtained on a Siemens D5000 instrument operating at 40 kV and 20 mA and using Cu Kα radiation (λ=0.15406 nm). The electrical conductivity of the carbon powders was determined on a home-made apparatus (four-probe method) by pressing the powders between two plungers into a hollow Nylon cylinder (inner diameter of 8 mm), and applying a pressure of 7.1 MPa. The vertical displacement of the plunger was measured by means of a manual cathetometer. In this way, the electrical conductivity and packing density can be

simultaneously determined. Elemental analysis (C, N and O) of the samples was carried out on a LECO CHN-932 microanalyzer.

2.3 Electrochemical measurements

Electrodes were prepared by mixing 85 wt % of active material, 10 wt % of polytetrafluoroethylene (PTFE) binder (Aldrich, 60 wt % suspension in water) and 5 wt % of the conductive additive Super C65 (Timcal company). The electrochemical measurements were performed in two-electrode Swagelok type cells. Electrochemical capacitors were assembled using two carbon electrodes of similar mass (mass loading ~ 5-10 mg cm^{-2}) and thickness (~100-150 µm), electrically isolated by a glassy fibrous separator. Stainless steel current collectors were used with 1 M $TEABF_4$/acetonitrile electrolyte and gold current collectors were employed with 1 M H_2SO_4 electrolyte. The electrochemical characterization was performed using a computer controlled potentiostat (Biologic VMP3 multichannel generator) and consisted of cyclic voltammetry, galvanostatic charge-discharge cycling experiments and electrochemical impedance spectroscopy measurements.

Galvanostatic charge/discharge tests were performed in the 0-2.5 V range in an organic medium and in the 0-1.1 V range in an aqueous medium at current densities in the 0.1 to 100 A g^{-1} range (based on the active mass of a single electrode). The specific gravimetric capacitance of a single electrode (F g^{-1}) determined from the galvanostatic cycles was calculated by means of the formula

$$C = \frac{2I}{\left(dV/dt\right) \times m}$$

where dV/dt = slope of the discharge curve (V s^{-1}). When non-linear voltage profiles were obtained owing to the presence of pseudocapacitance, best practice methods were followed for the calculation of the capacitance, *i.e.* the upper half of the discharge curve was used to determine the slope of the discharge curve [33, 34].

To trace the Ragone-like plots from the constant current discharge tests, the volumetric energy (Wh L^{-1}) and average power (kW L^{-1}) density were calculated using the following formulae:

$$E = \frac{1}{2} C_{cell} \Delta V_d^{\,2}$$

$$P = \frac{E}{\Delta t_d}$$

where C_{cell} is the volumetric capacitance of the total cell (F L^{-1}), ΔV_d is the operation voltage (V_{max} – IR_{drop}) and Δ_{td} is the discharge time.

Electrochemical impedance spectroscopy (EIS) was carried out at open-circuit voltage (*i.e.*, 0 V) within the frequency range of 1 mHz to 100 kHz and a 10 mV AC amplitude. Nyquist plots and plots of the dependence of capacitance on frequency were recorded to characterize the impedance of the tested samples. The specific gravimetric capacitance of a single electrode at each frequency, C_{EIS} (F/g), was calculated from the following formula and normalized with respect to the highest specific gravimetric capacitance, *i.e.* the specific gravimetric capacitance at the lowest frequency, *i.e.* 1 mHz:

$$C_{EIS} = \frac{2|Im(Z)|}{2\pi f \left[(Im(Z))^2 + (Re(Z))^2\right] \cdot m}$$

where f is the operating frequency (Hz), and $Im(Z)$ and $Re(Z)$ are the imaginary and real components of the total device resistance (Ohm). The relaxation time constant, τ_0, which defines the boundary between the regions of capacitive and resistive behaviors of the supercapacitor, was deduced from the frequency f_0 as follows: $\tau_0 = \frac{1}{f_0}$, where f_0 can be obtained from the real capacitance plot at $C' = \frac{C_{1mHz}}{2}$. The equivalent series resistance (ESR) was calculated from the intercept of the Nyquist plot with the real impedance axis at the highest frequency [35, 36]. The equivalent distributed resistance (EDR) was determined from the linear projection of the vertical portion at low frequencies to the real axis (after subtraction of the ESR) [35].

3. Results and Discussion

3.1 Structural and chemical properties

The structural characteristics of the N-doped carbon spheres were investigated by means of SEM, TEM and nitrogen physisorption techniques. The SEM and TEM images displayed in Figures 1a and 1b reveal that the templated carbon particles (N-CS-850 sample) consist of uniform microspheres with a smooth surface and a diameter of 1.2 ± 0.1 µm (see inset Figure 1a). The N_2 sorption isotherms and the pore size distributions (PSDs) of the templated carbon microspheres are displayed in Figure 2. The adsorption isotherms are of Type I which is characteristic of microporous materials. This is confirmed by the PSDs which show that the porosity is essentially made up of micropores (> 70 % of the pore volume) centered at around 1 nm. The textural properties summarized

in Table 1 reveal that the templated carbon possesses high BET surface areas in the 1190-1380 m^2 g^{-1} range and large pore volumes (0.61-0.74 cm^3 g^{-1}). Importantly, the porous carbon microspheres N-CS-850 exhibit a high packing density of 0.97 g cm^{-3}, which is similar to that reported by Yan et al. for a functionalized graphene with ultra-high volumetric performance [18], and higher than that of commercial activated carbons used in supercapacitors, such as Supra and Super DLC-50, i.e. ~ 0. 75 g cm^{-3}.

In order to increase the porosity of the templated carbon spheres and, in particular, the micropore volume, these materials were subjected to an additional activation process with KOH. As can be deduced by SEM inspection (Figures 1c and 1d), the chemical activation step induces a slight reduction in the diameter of the microspheres down to 0.95 ± 0.15 μm for N-CSA-700 (see inset in Fig. 1c) and to 1 ± 0.1 μm for N-CSA-600 (see inset in Figure 1d). However, the activated carbon spheres still retain their spherical morphology and a smooth surface appearance. A comparison of the N_2 sorption isotherms corresponding to the activated samples and the templated carbon is presented in Figure 2. As in the case of the templated carbons, the activated samples show a Type I isotherm although the nitrogen uptakes are considerably larger. These isotherms exhibit a sharp adsorption knee at low relative pressures, which reflects the microporous nature of the adsorbents. This is confirmed by the PSDs, which show that almost all the pores are below 2 nm in size (micropores). Moreover, it can be seen that the porosity is distributed into two micropore systems with sizes centered at 0.85 nm and 1.4 nm. Remarkably, whereas the porosity of the templated microspheres is formed by only one pore system of ~ 1 nm, the activated microspheres contain an additional micropore

system formed by narrower micropores of ~ 0.85 nm. These narrower micropores, which have been generated during the activation step, are highly relevant to the use of these materials for supercapacitor electrodes [12]. The textural properties listed in Table 1 show that the activation step has notably increased the BET surface area and the pore volume of the activated samples up to values of 2450 m^2 g^{-1} and 1.17 cm^3 g^{-1} in the case of N-CSA-700, and 2690 m^2 g^{-1} and 1.26 cm^3 g^{-1} in the case of N-CSA-600. In addition, the data included in Table 1 show that the micropore volume of the activated materials constitutes around 90 % of the total pore volume, thereby confirming that they are essentially microporous.

The nitrogen content of the templated carbon microspheres N-CS-850, as determined by elemental analysis, is 8.8 wt %. The chemical activation provokes a notable reduction in the nitrogen content down to ~ 2 wt % (N-CSA-600 and N-CSA-700). The chemical nature of the N-groups in the templated and activated microspheres was investigated by means of X-ray photoelectron spectroscopy (XPS) and the XPS N 1s core level spectra are displayed in Figure 3. These spectra can be deconvoluted into three peaks that are assigned to pyridinic nitrogen (N-6), quaternary nitrogen (N-Q) and pyridinic nitrogen oxide (N-O) [37, 38]. The relative abundance (%) of each N-group in the different samples is listed in Table 2. The results show that in both the templated and the activated samples, quaternary and pyridinic nitrogen groups are the most abundant nitrogen functionalities (> 85 %), whereas the N-O groups represent only < 15 %.

These carbon samples have a microstructure consisting of a disordered carbon framework, as can be deduced from the XRD patterns shown in Figure

S1 (Supporting Information). In the case of samples N-CS-850 and N-CSA-700, a sharp peak appears at around 2θ=26°, which is assigned to the *(002)* diffraction of graphitic carbon. This peak is superimposed on a broad band corresponding to amorphous carbon and it reveals the presence of a small fraction of graphitic carbon embedded inside an amorphous matrix. It results from the conversion of a small amount of amorphous carbon into more ordered carbon by the catalytic action of iron particles embedded inside the carbon matrix [39-43]. In the case of the sample carbonized at 600 ºC, only amorphous carbon was obtained.

As expected, a notable reduction in the packing density takes place when the carbon microspheres are activated. Indeed, whereas the N-CS-850 has a packing density of 0.97 g cm^{-3}, the activated samples exhibit values of 0.51 g cm^{-3} for N-CSA-700 and 0.59 g cm^{-3} in the case of N-CSA-600. However, despite this decrease, these values are still superior to those of other many carbon nanomaterials [7, 15]. Finally, it needs to be pointed out that the activated microspheres possess good electrical conductivities of 1.7 S cm^{-1} in the case of N-CSA-700 and 1.9 S cm^{-1} in the case of N-CSA-600, values which are even superior to that of the templated sample N-CS-850 (0.02 S cm^{-1}).

3.2 Electrochemical characterization

The electrochemical capacitive properties of the N-doped microspheres were measured in aqueous (1 M H_2SO_4) and organic (1 M 1 M $TEABF_4$/AN) electrolytes. As a first step, to evaluate the charge transport within the pore structure of these materials, EIS measurements were performed in the discharge state. Figure 4 shows the corresponding Nyquist plots and the frequency-dependence of capacitance. At first glance, a large 45º Warburg

region, indicating substantial resistance to the diffusion of ions within the porous structure (resistance known as EDR), can be identified in H_2SO_4 in Figure 4a in the case of the N-CS-850-based supercapacitor (5.6 Ω), whereas it is almost negligible in the activated N-CSA-600- and N-CSA-700-based supercapacitors (*i.e.* 0.04 and 0.05 Ω respectively) owing to the more extended development of their porosity and enlarged pore size. Besides, the value of ESR (equivalent series resistance) of the activated microsphere-based supercapacitors (0.17 and 0.21 Ω) is half that of the pristine microsphere-based supercapacitor (0.53 Ω), which is a clear consequence of the higher electronic conductivity of the activated microspheres (see above). These low values of ESR and EDR will lead to a small trade-off between energy and power, as will be shown later in a Ragone-like plot. In organic electrolyte, an increase in both ESR and EDR (Figure 4c) is observed for all the materials, as might be expected given the lower conductivity and the larger size of the ions of this electrolyte in comparison to those of aqueous H_2SO_4. It was found that the activated microspheres possess small relaxation time constants in the 0.42-0.66 s range in H_2SO_4 electrolyte, as can be deduced from the variation of normalized capacitance with frequency (see Figure 4b). These values are lower than those of many carbons found in the literature, such as meso- and microporous carbon materials [44], three-dimensionally hierarchical porous carbon [45], activated graphite oxide [23], and vertically aligned reduced graphene oxide [46]. On the other hand, as expected, the relaxation time constants of the activated microspheres in $TEABF_4$/AN electrolyte (3.8 s and 7.1 s for N-CSA-600 and N-CSA-700, respectively) are superior to those obtained in aqueous electrolyte (see Figure 4d). As can be inferred from the results presented in Figures 4b and

4d, the relaxation time constants measured for the activated microspheres are considerably smaller than those obtained for the pristine microspheres (*i.e*. 6.7 s in H_2SO_4 electrolyte and 12.5 s in $TEABF_4$/AN electrolyte), which will lead to a better rate capability as shown below.

The electrochemical behavior of the carbon microspheres in aqueous electrolyte (1 M H_2SO_4) was investigated in a two-electrode system by means of charge-discharge (CD) and cyclic voltammetry (CV) experiments. Figures 5a-c show the CD profiles obtained at different current densities in the 0.5-100 A g^{-1} range. In the case of the N-CS-850 sample, the voltage profiles (see Figures 5a and 5b) are non-linear, which suggests redox reactions associated to the presence of N-groups, more specifically to the presence of pyridinic-N, which is involved in proton exchange redox reactions [47-50]. These pseudocapacitive effects are also evident in the cyclic voltammograms depicted in Figure S2a. On the other hand, the activated carbon microspheres, which have low nitrogen contents, exhibit a nearly constant slope, reflecting the absence of major pseudocapacitive effects. This behavior is confirmed by the cyclic voltammograms represented in Figures S2b and S2c. It can be observed that, whereas the templated microspheres N-CS-850 exhibit a large resistance (*i.e.* large IR drop) at high current densities (see Figure S2d), the activated samples exhibit a remarkably low IR drop even at an ultra-high discharge current density of 100 A g^{-1}, as can be seen in Figure 5c. This behavior is a consequence of the fact that the activated samples have low ion-transport resistances as well as a relatively high electronic conductivity, which is in agreement with the EIS measurements (*vide supra*). The excellent rate performance at high discharge current densities is confirmed by the results displayed in Figure 5d, which show

the variation in specific capacitance *versus* current density. Thus, the activated carbon microspheres have specific capacitances at a low discharge rate of 0.1 A g^{-1} of 310 and 260 F g^{-1} in the case of N-CSA-600 and N-CSA-700 respectively. More importantly, at an ultra-high current density of 100 F g^{-1} they still retain a specific capacitance of 178 F g^{-1} (57%) and 138 F g^{-1} (53 %) for N-CSA-600 and N-CSA-700 respectively. In the case of the templated N-doped microspheres N-CS-850, it is important to note that, despite having a specific surface area which is half that of N-CSA-600 and N-CSA-700, they possess an impressive specific capacitance of 297 F g^{-1} which can be ascribed to the large contribution of pseudocapacitance associated to the N-groups. Thus, a surface area-normalized capacitance of 23.2 μF m^{-2} is recorded for N-CS-850 *vs.* 10.6 and 11.5 μF m^{-2} for N-CSA-700 and N-CSA-600 respectively. However, due to the fact that the non-activated microspheres N-CS-850 exhibit a high resistance to the movement of ions within the porous structure (*vide supra*), they are able to work only up to 40 A·g^{-1} with a 50 % of capacitance fading (see Figure 5d). The positive effect of KOH activation upon capacitive performance at high current densities can be ascribed to the widening of micropores and the increase in porosity, which notably improves ion transport within the pore network. Nevertheless, it should be noted that, despite a lower capacitance retention, the pristine N-doped microspheres still exhibit a better rate performance than many advanced carbons found in the literature such as three-dimensionally hierarchical porous carbon [45], ordered mesoporous carbon nanopipes with nitrogen species [50], N-doped graphene sheets [51], N-rich carbon nanotubes composites [52] and N-doped carbon nanospheres [53]. The stability of the carbon microsphere-based supercapacitors was evaluated by

long-term charge-discharge cycling at a current density of 5 A g^{-1} over 5000 cycles (Figure 5e). It can be seen that about 96-98 % of specific capacitance was retained in all cases, which is proof of an excellent cycling stability.

As a consequence of their high packing densities, the carbon microspheres exhibit large volumetric capacitances, as shown in Figure 5d. Especially remarkable is the case of the templated N-doped carbon microspheres N-CS-850 (packing density: 0.97 g cm^{-3}), whose volumetric capacitance is very close to the gravimetric one, with a value of 287 F cm^{-3} (at 0.1 A g^{-1}), which is one of the highest values ever reported (see Table S1). On the other hand, the activated carbon spheres, with lower packing densities (*i.e.* 0.59 g cm^{-3} for N-CSA-600 and 0.51 g cm^{-3} for N-CSA-700) still exhibit high volumetric capacitances which are comparable, or superior, to most of the values reported in the literature (see Table S1). Figure 5f provides a comparison of the volumetric power and energy densities of the different materials. Especially remarkable is the behavior of the N-CS-850 sample which exhibits a very high volumetric energy density of 12 Wh L^{-1} at an average power density of 0.04 kW L^{-1} while the average power density even reaches 19 kW L^{-1} for an energy density of 4.4 Wh L^{-1}. A comparison of the volumetric performance of the (N-CS-850)-based supercapacitor with that deduced for other materials reported in the literature is provided in Figure S4. It can be seen that the data reported here for the N-CS-850 sample are among the best values reported so far for carbon materials in aqueous electrolytes. Worthy of special note is the fact that, although N-CS-850 does not possess a high volumetric energy density at low rates, this material can deliver much more energy than

other materials at high rates, which, after all, is the ultimate aim of supercapacitors.

The electrochemical performance of the porous carbon microspheres was also evaluated in an organic electrolyte, *i.e.* 1 M $TEABF_4$/AN, using a two-electrode cell system. Figure 6a shows the galvanostatic charge/discharge voltage profiles at 0.5 $A \cdot g^{-1}$ and up to 2.5 V. They are highly linear and symmetrical (coulombic efficiency ~ 98 %), indicating an efficient double-layer energy storage mechanism and an absence of pseudocapacitance phenomena. This is confirmed by the cyclic voltammograms shown in Figure S3. It should be noted that the activated microspheres N-CSA-600 and N-CSA-700 are stable up to a cell voltage of 2.5 V, whereas the non-activated N-CS-850 sample only just reaches 2 V. This is clearly illustrated by the cyclic voltammograms represented in Figures S3c and S3d. Figure 6b shows the variation in specific capacitance with current density for all the samples. It can be seen that at a low discharge rate of 0.1 A g^{-1} the activated samples exhibit high specific capacities (*i.e.* 144 F g^{-1} for N-CSA-700 and 154 F g^{-1} for N-CSA-600), considerably higher than that attained by the non-activated N-CS-850 sample (110 F g^{-1}), which is in agreement with the differences in pore development. At this point, it should be noted that these activated carbon spheres exhibit high volumetric capacitances (92 F cm^{-3} for N-CSA-600 and 74 F cm^{-3} for N-CSA-700) which are similar, or even superior, to those of many carbon materials reported in the literature (see Table S2).

The above results show that, whereas the N-doped microspheres are advantageous in aqueous electrolyte due to their pseudocapacitance effects, in organic electrolyte, where redox reactions involving the N-groups do not take

place, highly porous materials with appropriate pore size distributions are more suitable. Besides, a lower voltage stability window is achieved with the N-doped microspheres, which may be ascribed to side reactions with the organic electrolyte, as observed for other highly functionalized materials [54]. Furthermore, in organic electrolyte the capacitance retention of the activated microspheres is very good, *i.e*. 83 % in the case of N-CSA-600 and 74 % for N-CSA-700 at 40 A g^{-1}. In contrast, the N-CS-850 sample could only just work at discharge currents up to 10 A g^{-1}. This behavior is in accordance with its low electronic conductivity and resistance to ion transport within the porous structure as was confirmed in the EIS measurements (see Figure 4c). The rate capability of the activated microspheres compares well with that of advanced porous carbons, including hierarchical porous carbons [55-58]. The stability of these materials in organic electrolyte was evaluated by charge-discharge cycling at 5 A g^{-1} over 5000 cycles in a working voltage window of 2.5 V. The results, displayed in Figure 6c, reveal that the capacitance retention of the activated microspheres is around 90 %, which demonstrates the robustness and stability of the electrode materials.

The Ragone-like plot in Figure 6d compares the energy-power characteristics of the N-CS-850 sample and the activated samples N-CSA-600 and N-CSA-700 at their maximum working voltage window in volumetric units. In the case of the activated microspheres, the high specific surface area and large working voltage window lead to a higher volumetric energy density than that of the non-activated carbon, despite having a much lower packing density. In this respect, the (N-CSA-600)-based supercapacitor exhibits the best energy and power characteristics in both gravimetric and volumetric units. For example,

it has a very high volumetric energy density of 16.6 Wh L^{-1}/33 Wh kg^{-1} for an average power density of 0.04 kW L^{-1}/0.06 kW kg^{-1} while the average power density reaches 13.6 kW L^{-1}/23.2 kW kg^{-1} for an energy density of 8.7 Wh L^{-1}/14.9 Wh kg^{-1}. A comparison of the volumetric energy and power characteristics of the activated carbon microspheres N-CSA-600 with the values deduced for different materials found in the literature is provided in Figure S5. It can be seen that the N-CSA-600 sample exhibits the best performance, delivering much more energy at high power densities than many advanced carbon materials found in the literature.

4. Conclusions

In summary, we have described a highly efficient and novel procedure for the fabrication of uniform porous carbon microspheres (diameter ~ 1 μm) that combine several important properties: a) a large number of nitrogen functional groups (up to 8.8 wt % N), b) a well-developed porosity made up of micropores with a BET surface area of 1280 m^2 g^{-1} and c) a high packing density of 0.97 g cm^{-3}. These N-doped carbon microspheres were synthesized using a nanocasting approach with pyrrole as carbon precursor and porous silica particles as sacrificial template. By means of an additional KOH activation step, the textural properties of the templated carbon were notably enhanced, the resulting activated samples exhibiting a bimodal microporosity and a BET surface area of up to 2690 m^2 g^{-1}. The high packing density of the carbon microspheres led to high volumetric capacitances, which are among the highest reported to date. Thus, values as high as ~ 290 F cm^{-3} in 1 M H_2SO_4 and ~ 90 F cm^{-3} in $TEABF_4$/AN were obtained in the case of the pristine microspheres and the microspheres activated at 600 ºC respectively. The pristine N-doped carbon microspheres exhibited the best performance in H_2SO_4 due to the pseudocapacitive contribution of the N-groups, providing high volumetric energy (up to 12 Wh L^{-1}) and power (up to 19 kW L^{-1}) densities. On the other hand, in organic electrolyte, where the charge storage mechanism is based on the formation of the electric double-layer, the activated carbon spheres performed better due to their larger specific surface area. Thus, they were able to store ~ 15 W h L^{-1} at an average power density of *ca*. 4 kW L^{-1}.

Acknowledgments. This research work was supported by Spanish Ministerio de Economía y Competitividad, MINECO (MAT2012-31651), and Fondo Europeo de Desarrollo Regional (FEDER). G. A. F. thanks the MINECO for his predoctoral contract and M. S. thanks the Spanish Ministerio de Ciencia e Innovación for her Ramón y Cajal contract.

Table 1. Textural properties of the N-doped microporous carbon microspheres.

Sample Code	S_{BET} ($m^2\ g^{-1}$)	V_p ($cm^3\ g^{-1}$)[a]	V_{mi} ($cm^3\ g^{-1}$)[b]	V_{meso} ($cm^3\ g^{-1}$)[c]	S_{mi} ($m^2\ g^{-1}$)[b]	N (wt %)
N-CS-850	1280	0.67	0.51	0.16	1060	8.8
N-CS-700	1380	0.74	0.53	0.21	1040	12.57
N-CS-600	1190	0.61	0.48	0.13	1030	14.44
N-CSA-850	1680	0.85	0.69	0.16	1620	1.95
N-CSA-700	2450	1.17	1.03	0.14	2190	2.04
N-CSA-600	2690	1.26	1.13	0.13	2280	1.86

[a] Pore volume determined at p/p_0=0.90. [b] The micropore volume and the micropore surface area were obtained by the QSDFT method. [c] The mesopore volume obtained from the difference between the pore volume (V_p) and micropore volume (V_{mi}).

Table 2. Relative amounts of the nitrogen functional groups as deduced by XPS measurements.

Sample Code	Nitrogen functional groups (%)		
	Pyridinic N (N-6)	Quaternary N (N-Q)	Pyridine-N-oxide (N-O)
N-CS-850	36.1	57.7	6.2
N-CSA-700	43.0	48.7	8.3
N-CSA-600	19.8	65.6	14.6

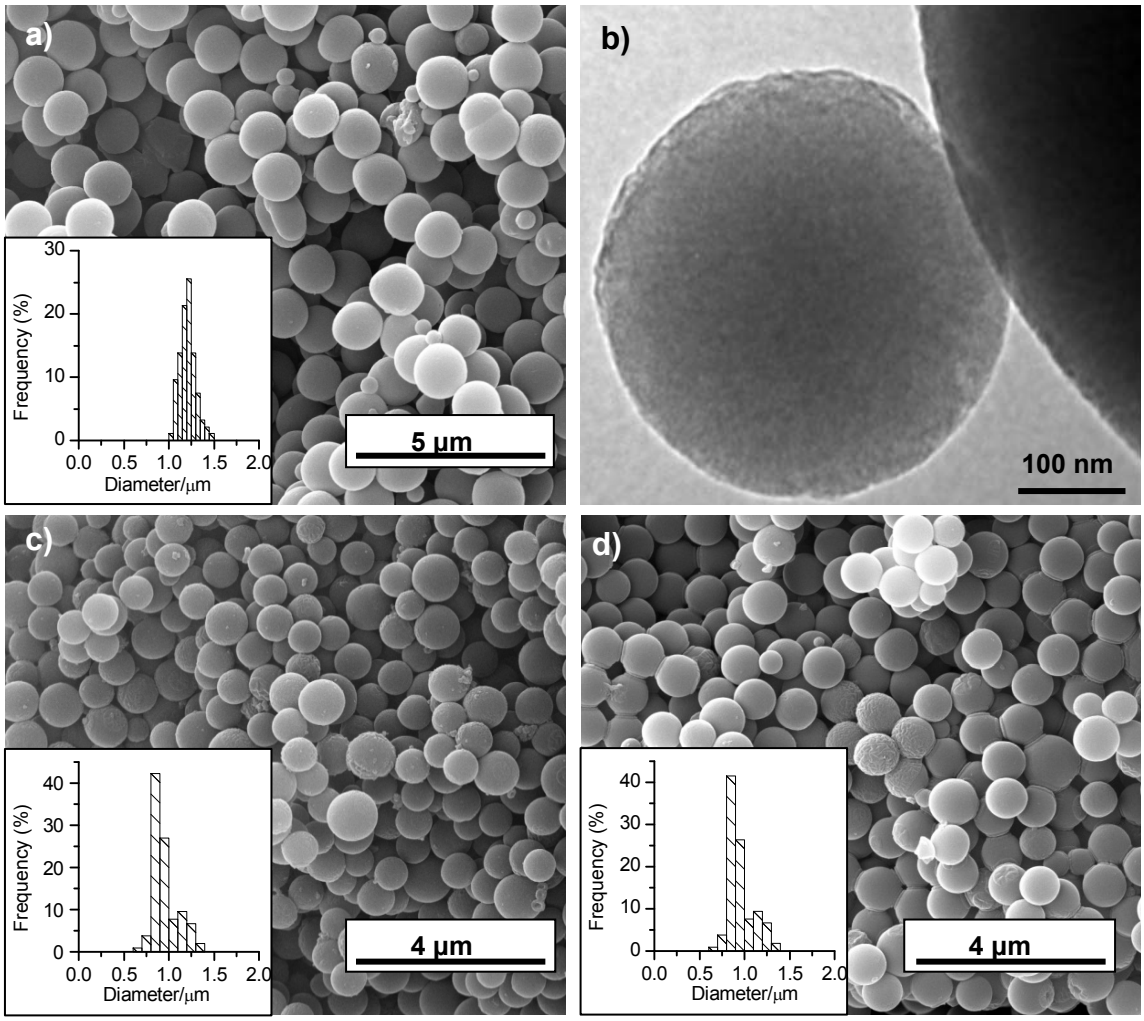

Figure 1. (a) SEM image and (b) TEM image of the N-doped carbon spheres N-CS-850, and SEM images of the activated N-doped carbon spheres (c) N-CSA-700 and (d) N-CSA-600. The insets in the SEM images display the particle diameter distribution.

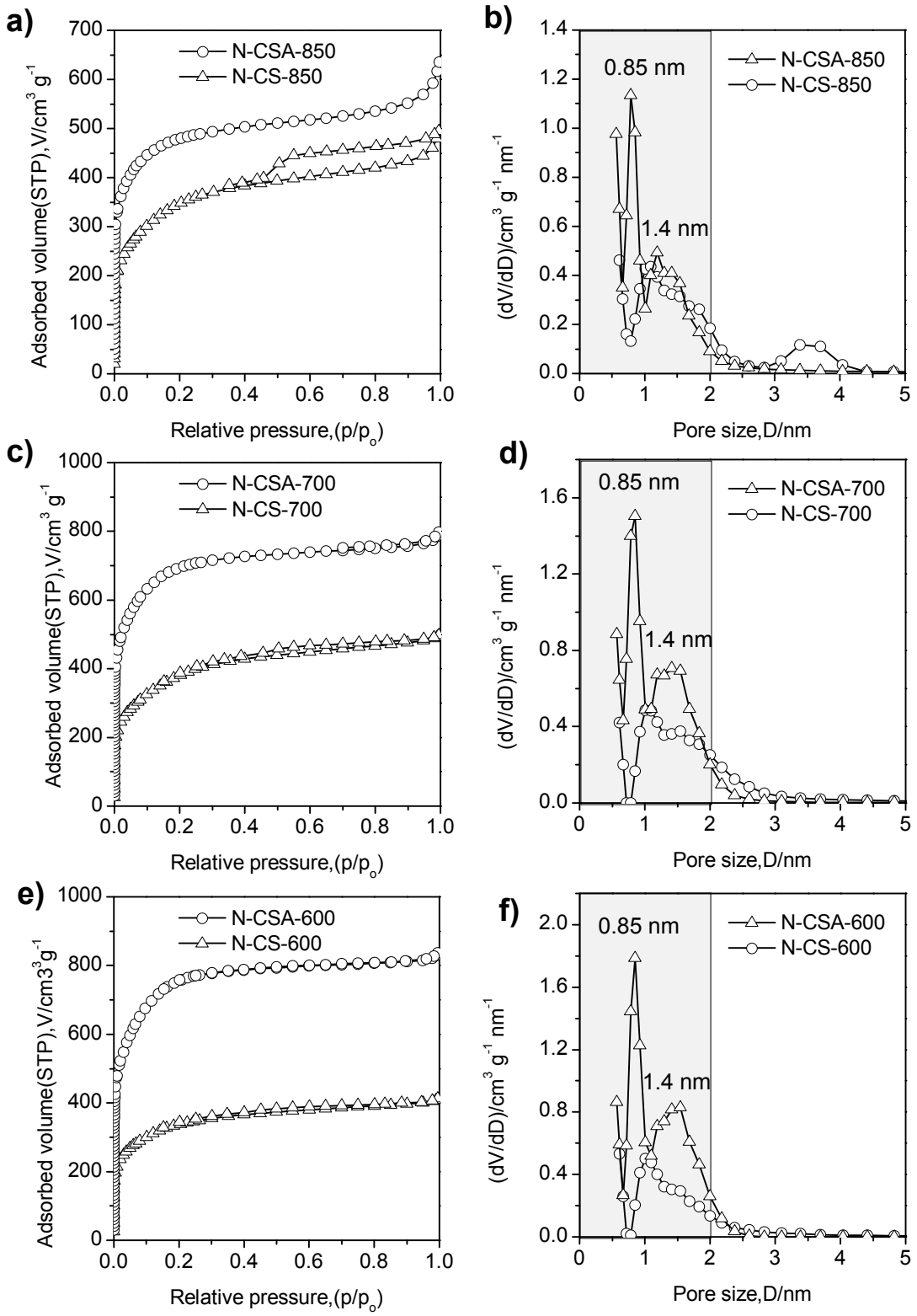
a)
N-CSA-850
N-CS-850
Adsorbed volume(STP),V/cm3 g-1
Relative pressure,(p/po)
b)
0.85 nm
1.4 nm
N-CSA-850
N-CS-850
(dV/dD)/cm3 g-1 nm-1
Pore size,D/nm
c)
N-CSA-700
N-CS-700
Adsorbed volume(STP),V/cm3 g-1
Relative pressure,(p/po)
d)
0.85 nm
1.4 nm
N-CSA-700
N-CS-700
(dV/dD)/cm3 g-1 nm-1
Pore size,D/nm
e)
N-CSA-600
N-CS-600
Adsorbed volume(STP),V/cm3g-1
Relative pressure,(p/po)
f)
0.85 nm
1.4 nm
N-CSA-600
N-CS-600
(dV/dD)/cm3 g-1 nm-1
Pore size,D/nm

Figure 2. Nitrogen sorption isotherms (a, c and e) and pore size distributions (b, d and f) calculated by QSDFT method for the N-doped carbon microspheres. The grey region in (b), (d) and (f) corresponds to the micropore range.

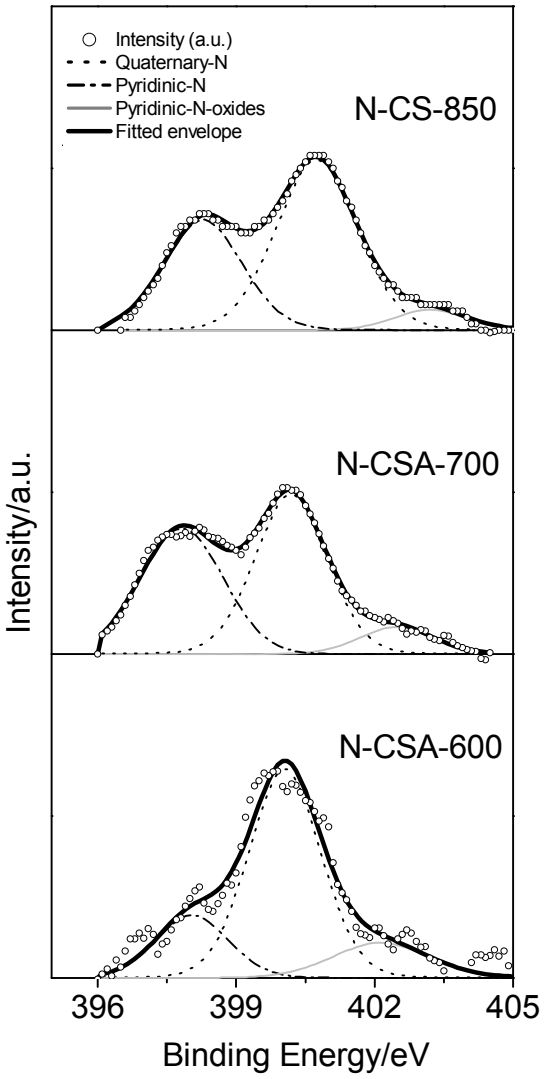

Figure 3. XPS N 1s core level spectra the N-doped carbon samples.

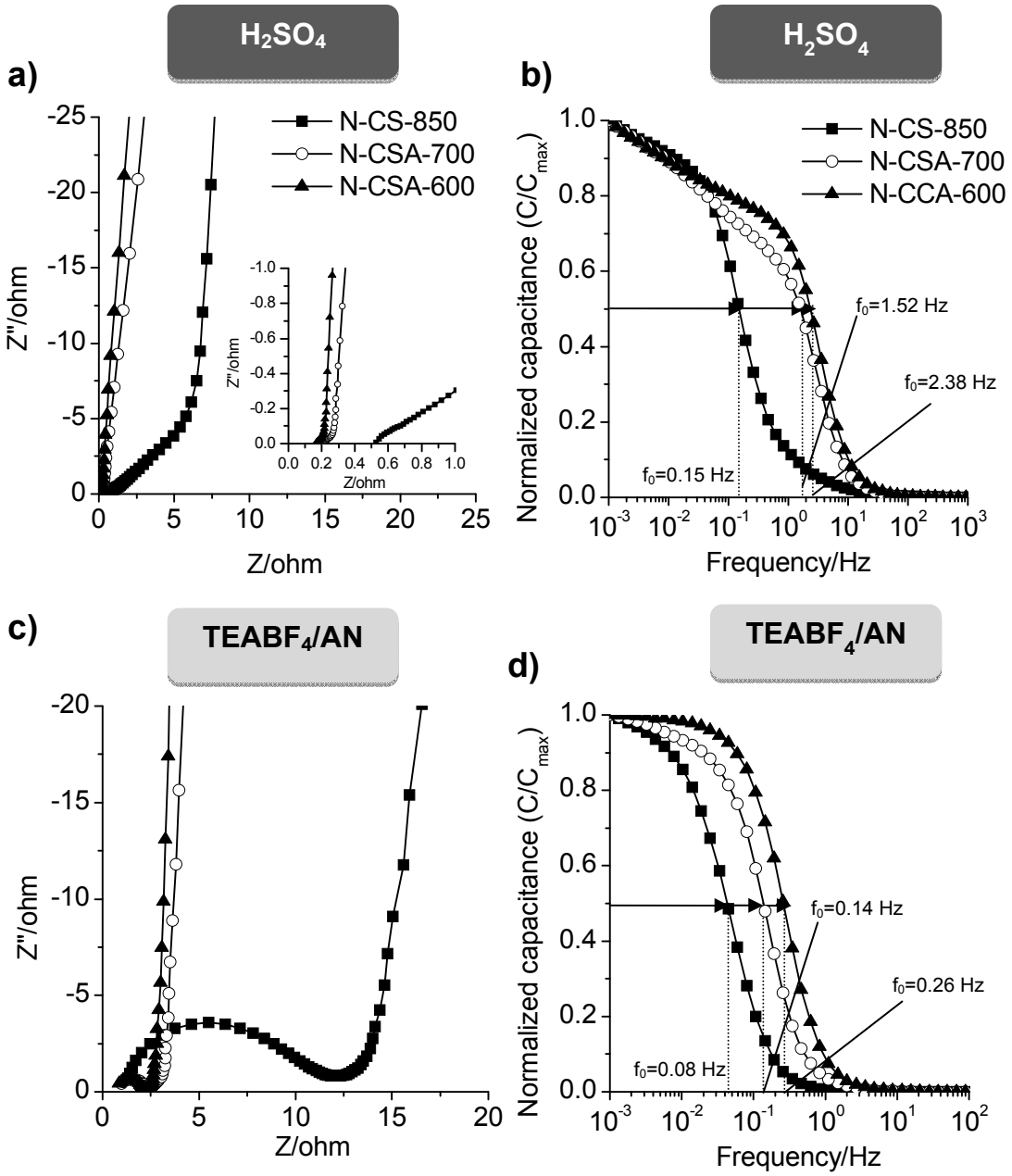

Figure 4. (a and c) Nyquist plots for the H_2SO_4 electrolyte (inset: Nyquist plot magnification), and the $TEABF_4$/AN electrolyte respectively; b and d) frequency response in the H_2SO_4 electrolyte and $TEABF_4$/AN electrolyte respectively.

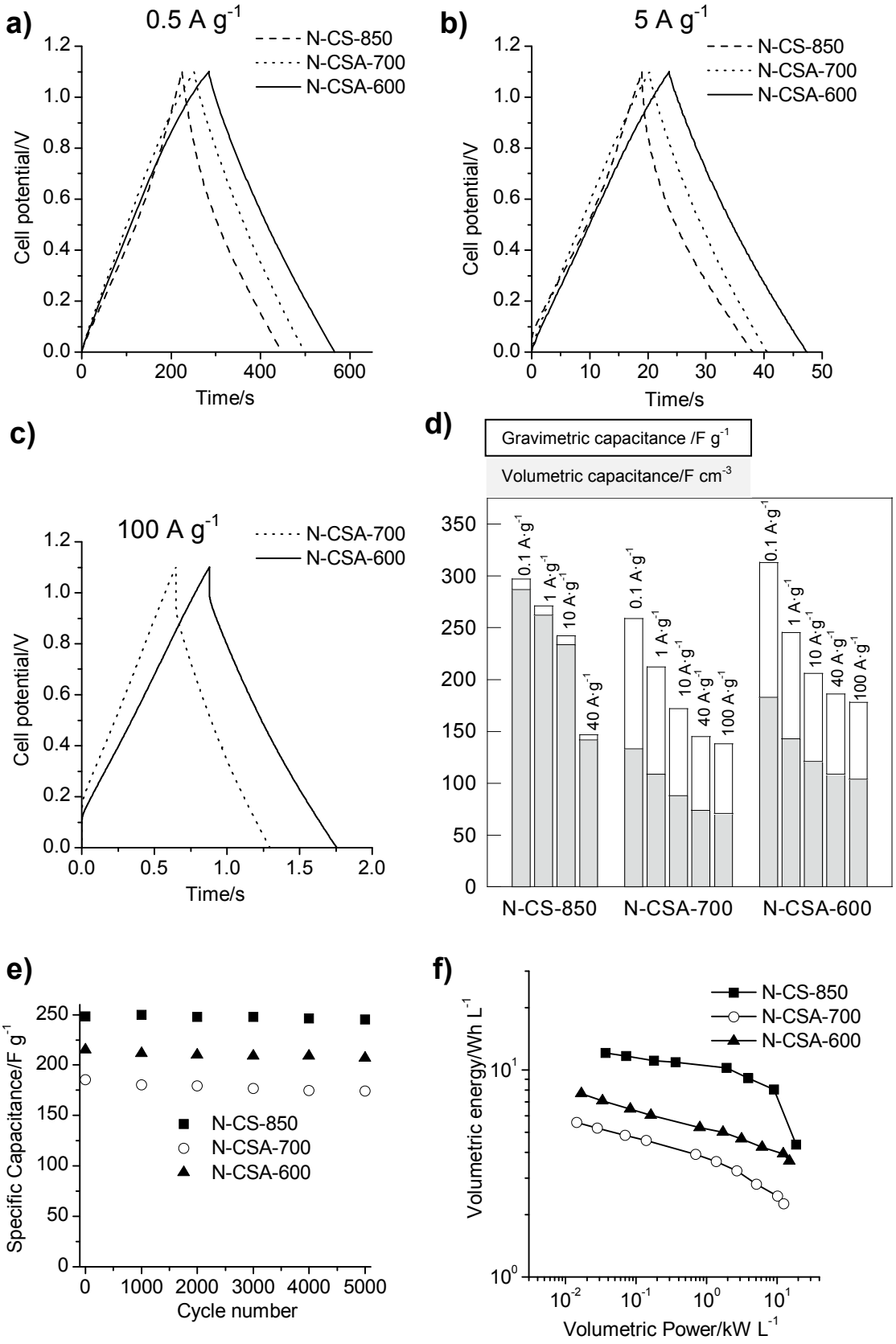

Figure 5. Galvanostatic charge-discharge voltage profiles at (a) 0.5 A g^{-1}, (b) 5 A g^{-1} and (c) 100 A g^{-1}; (d) variation of the gravimetric and volumetric

capacitance with increasing current density; (e) long-term stability under cycling at 5 A g^{-1} and (f) Ragone-like plot in volumetric units corresponding to the N-doped microspheres. Electrolyte: 1 M H_2SO_4, cell voltage = 1.1 V.

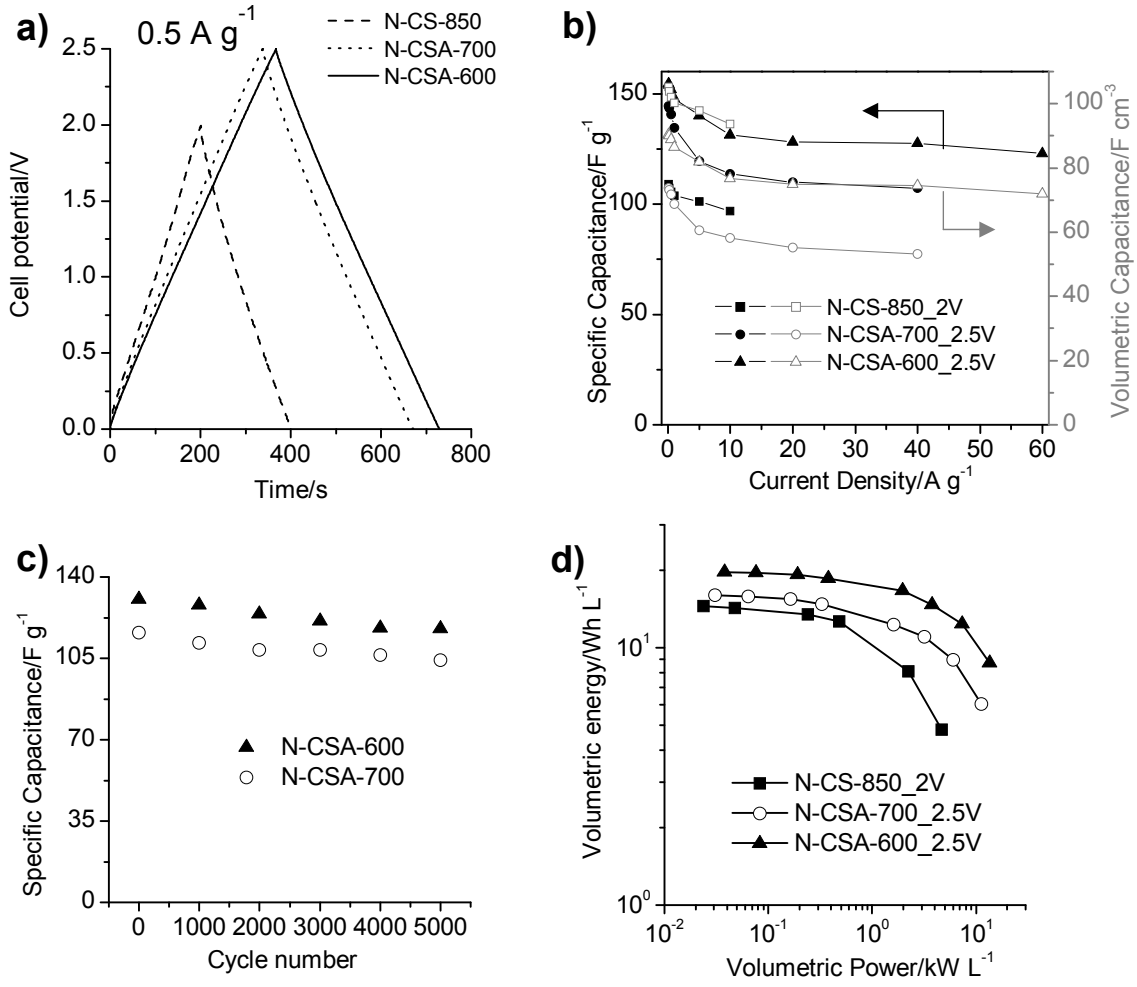

Figure 6. (a) Galvanostatic charge/discharge voltage profiles at 0.5 A g^{-1}, (b) rate-dependence of the specific capacitance (black color) and volumetric capacitance (grey color), (c) long-term stability under cycling at 5 A g^{-1} and (d) Ragone-like plot in volumetric units, corresponding to the N-doped microspheres. Electrolyte: 1 M $TEABF_4$/AN, cell voltage = 2.5 V for N-CSA-700 and N-CSA-600; and cell voltage = 2 V for N-CS-850.

References

[1] B.E. Conway, Electrochemical Supercapacitors, Scientific Fundamentals and Technological Applications, 1999.

[2] Elzbieta Frackowiak, F. Beguin, Carbon materials for the electrochemical storage of energy in capacitors, Carbon, 39 (2001) 937.

[3] F. Beguin, V. Presser, A. Balducci, E. Frackowiak, Supercapacitors: carbons and electrolytes for advanced supercapacitors, Adv Mater, 26 (2014) 2283.

[4] A. Ghosh, Y.H. Lee, Carbon-Based Electrochemical Capacitors, ChemSusChem, 5 (2012) 480-499.

[5] G. Wang, L. Zhang, J. Zhang, A review of electrode materials for electrochemical supercapacitors, Chem. Soc. Rev., 41 (2012) 797-828.

[6] E. Frackowiak, Carbon materials for supercapacitor application, Phys. Chem. Chem. Phys., 9 (2007) 1774-1785.

[7] W. Gu, G. Yushin, Review of nanostructured carbon materials for electrochemical capacitor applications: advantages and limitations of activated carbon, carbide-derived carbon, zeolite-templated carbon, carbon aerogels, carbon nanotubes, onion-like carbon, and graphene, Wiley Interdisciplinary Reviews: Energy and Environment, 3 (2014) 424-473.

[8] A. Stein, Z. Wang, M.A. Fierke, Functionalization of Porous Carbon Materials with Designed Pore Architecture, Adv. Mater., 21 (2009) 265-293.

[9] A.G. Pandolfo, A.F. Hollenkamp, Carbon properties and their role in supercapacitors, J. Power Sources, 157 (2006) 11-27.

[10] F. Ma, H. Zhao, L. Sun, Q. Li, L. Huo, T. Xia, S. Gao, G. Pang, Z. Shi, S. Feng, A facile route for nitrogen-doped hollow graphitic carbon spheres with

superior performance in supercapacitors, J. Mater. Chem., 22 (2012) 13464-13468.

[11] C.O. Ania, V. Khomenko, E. Raymundo-Piñero, J.B. Parra, F. Béguin, The Large Electrochemical Capacitance of Microporous Doped Carbon Obtained by Using a Zeolite Template, Adv. Funct. Mater., 17 (2007) 1828-1836.

[12] P. Simon, Y. Gogotsi, Capacitive Energy Storage in Nanostructured Carbon–Electrolyte Systems, Acc. Chem. Res., 46 (2012) 1094-1103.

[13] M. Beidaghi, Y. Gogotsi, Capacitive energy storage in micro-scale devices: recent advances in design and fabrication of micro-supercapacitors, Energy Environ. Sci., 7 (2014) 867-884.

[14] Z.-S. Wu, K. Parvez, A. Winter, H. Vieker, X. Liu, S. Han, A. Turchanin, X. Feng, K. Müllen, Layer-by-Layer Assembled Heteroatom-Doped Graphene Films with Ultrahigh Volumetric Capacitance and Rate Capability for Micro-Supercapacitors, Adv. Mater., 26 (2014) 4552-4558.

[15] Y. Gogotsi, P. Simon, True Performance Metrics in Electrochemical Energy Storage, Science, 334 (2011) 917-918.

[16] N. Jung, S. Kwon, D. Lee, D.-M. Yoon, Y.M. Park, A. Benayad, J.-Y. Choi, J.S. Park, Synthesis of Chemically Bonded Graphene/Carbon Nanotube Composites and their Application in Large Volumetric Capacitance Supercapacitors, Adv. Mater., 25 (2013) 6854-6858.

[17] J. Yan, Q. Wang, T. Wei, L. Jiang, M. Zhang, X. Jing, Z. Fan, Template-Assisted Low Temperature Synthesis of Functionalized Graphene for Ultrahigh Volumetric Performance Supercapacitors, ACS Nano, 8 (2014) 4720-4729.

[18] J. Yan, Q. Wang, C. Lin, T. Wei, Z. Fan, Interconnected Frameworks with a Sandwiched Porous Carbon Layer/Graphene Hybrids for Supercapacitors with

High Gravimetric and Volumetric Performances, Adv. Energy Mater., (2014) DOI: 10.1002/aenm.201400500.

[19] M. Ghaffari, Y. Zhou, H. Xu, M. Lin, T.Y. Kim, R.S. Ruoff, Q.M. Zhang, High-Volumetric Performance Aligned Nano-Porous Microwave Exfoliated Graphite Oxide-based Electrochemical Capacitors, Adv. Mater., 25 (2013) 4879-4885.

[20] X. Yang, C. Cheng, Y. Wang, L. Qiu, D. Li, Liquid-Mediated Dense Integration of Graphene Materials for Compact Capacitive Energy Storage, Science, 341 (2013) 534-537.

[21] J. Chmiola, C. Largeot, P.-L. Taberna, P. Simon, Y. Gogotsi, Monolithic Carbide-Derived Carbon Films for Micro-Supercapacitors, Science, 328 (2010) 480-483.

[22] Y. Tao, X. Xie, W. Lv, D.-M. Tang, D. Kong, Z. Huang, H. Nishihara, T. Ishii, B. Li, D. Golberg, F. Kang, T. Kyotani, Q.-H. Yang, Towards ultrahigh volumetric capacitance: graphene derived highly dense but porous carbons for supercapacitors, Sci. Rep., 3 (2013).

[23] S. Murali, N. Quarles, L.L. Zhang, J.R. Potts, Z. Tan, Y. Lu, Y. Zhu, R.S. Ruoff, Volumetric capacitance of compressed activated microwave-expanded graphite oxide (a-MEGO) electrodes, Nano Energy, 2 (2013) 764-768.

[24] L.L. Zhang, Y. Gu, X.S. Zhao, Advanced porous carbon electrodes for electrochemical capacitors, J. Mater. Chem. A, 1 (2013) 9395-9408.

[25] W. Xiong, M. Liu, L. Gan, Y. Lv, Y. Li, L. Yang, Z. Xu, Z. Hao, H. Liu, L. Chen, A novel synthesis of mesoporous carbon microspheres for supercapacitor electrodes, J. Power Sources, 196 (2011) 10461-10464.

[26] X. Wang, L. Liu, X. Wang, L. Bai, H. Wu, X. Zhang, L. Yi, Q. Chen, Preparation and performances of carbon aerogel microspheres for the application of supercapacitor, J. Solid State Electrochem., 15 (2011) 643-648.

[27] M.-X. Liu, L.-H. Gan, W. Xiong, D.-Z. Zhu, Z.-J. Xu, L.-W. Chen, Partially graphitic micro- and mesoporous carbon microspheres for supercapacitors, Chin. Chem. Lett., 24 (2013) 1037-1040.

[28] F. Su, C.K. Poh, J.S. Chen, G. Xu, D. Wang, Q. Li, J. Lin, X.W. Lou, Nitrogen-containing microporous carbon nanospheres with improved capacitive properties, Energy Environ. Sci., 4 (2011) 717-724.

[29] S. Tanaka, H. Nakao, T. Mukai, Y. Katayama, Y. Miyake, An Experimental Investigation of the Ion Storage/Transfer Behavior in an Electrical Double-Layer Capacitor by Using Monodisperse Carbon Spheres with Microporous Structure, J. Phys. Chem. C, 116 (2012) 26791-26799.

[30] M. Liu, L. Gan, W. Xiong, Z. Xu, D. Zhu, L. Chen, Development of MnO2/porous carbon microspheres with a partially graphitic structure for high performance supercapacitor electrodes, J. Mater. Chem. A, 2 (2014) 2555-2562.

[31] R.I. Nooney, D. Thirunavukkarasu, Y. Chen, R. Josephs, A.E. Ostafin, Synthesis of Nanoscale Mesoporous Silica Spheres with Controlled Particle Size, Chem. Mater., 14 (2002) 4721-4728.

[32] T. Kim, G. Jung, S. Yoo, K.S. Suh, R.S. Ruoff, Activated Graphene-Based Carbons as Supercapacitor Electrodes with Macro- and Mesopores, ACS Nano, 7 (2013) 6899-6905.

[33] M.D. Stoller, R.S. Ruoff, Best practice methods for determining an electrode material's performance for ultracapacitors, Energy Environ. Sci., 3 (2010) 1294-1301.

[34] S. Zhang, N. Pan, Supercapacitors Performance Evaluation, Adv. Energy Mater., 5 (2015) DOI: 10.1002/aenm.201401401.

[35] R. Kötz, M. Carlen, Principles and applications of electrochemical capacitors, Electrochim. Acta, 45 (2000) 2483-2498.

[36] C. Portet, P.L. Taberna, P. Simon, C. Laberty-Robert, Modification of Al current collector surface by sol–gel deposit for carbon–carbon supercapacitor applications, Electrochim. Acta, 49 (2004) 905-912.

[37] J.R. Pels, F. Kapteijn, J.A. Moulijn, Q. Zhu, K.M. Thomas, Evolution of nitrogen functionalities in carbonaceous materials during pyrolysis, Carbon, 33 (1995) 1641-1653.

[38] H. Schmiers, J. Friebel, P. Streubel, R. Hesse, R. Köpsel, Change of chemical bonding of nitrogen of polymeric N-heterocyclic compounds during pyrolysis, Carbon, 37 (1999) 1965-1978.

[39] M. Sevilla, A.B. Fuertes, Catalytic graphitization of templated mesoporous carbons, Carbon, 44 (2006) 468-474.

[40] M. Sevilla, C. Sanchis, T. Valdes-Solis, E. Morallon, A.B. Fuertes, Synthesis of graphitic carbon nanostructures from sawdust and their application as electrocatalyst supports, J. Phys. Chem. C, 111 (2007) 9749-9756.

[41] A. Ōya, H. Marsh, Phenomena of catalytic graphitization, J. Mater. Sci., 17 (1982) 309-322.

[42] H. Marsh, D. Crawford, D.W. Taylor, Catalytic graphitization by iron of isotropic carbon from polyfurfuryl alcohol, 725–1090 K. A high resolution electron microscope study, Carbon, 21 (1983) 81-87.

[43] J. Ozaki, M. Mitsui, Y. Nishiyama, Carbonization of ferrocene containing polymers and their electrochemical properties, Carbon, 36 (1998) 131-135.

[44] J. Yin, D. Zhang, J. Zhao, X. Wang, H. Zhu, C. Wang, Meso- and micro-porous composite carbons derived from humic acid for supercapacitors, Electrochim. Acta, 136 (2014) 504-512.

[45] Y. Han, S. Liu, D. Li, X. Li, Three-dimensionally Hierarchical Porous Carbon Creating High-performance Electrochemical Capacitors, Electrochim. Acta, 138 (2014) 193-199.

[46] Y. Yoon, K. Lee, S. Kwon, S. Seo, H. Yoo, S. Kim, Y. Shin, Y. Park, D. Kim, J.-Y. Choi, H. Lee, Vertical Alignments of Graphene Sheets Spatially and Densely Piled for Fast Ion Diffusion in Compact Supercapacitors, ACS Nano, 8 (2014) 4580-4590.

[47] G. Lota, K. Lota, E. Frackowiak, Nanotubes based composites rich in nitrogen for supercapacitor application, Electrochem. Commun., 9 (2007) 1828-1832.

[48] Y.-H. Lee, K.-H. Chang, C.-C. Hu, Differentiate the pseudocapacitance and double-layer capacitance contributions for nitrogen-doped reduced graphene oxide in acidic and alkaline electrolytes, J. Power Sources, 227 (2013) 300-308.

[49] D.-W. Wang, F. Li, L.-C. Yin, X. Lu, Z.-G. Chen, I.R. Gentle, G.Q. Lu, H.-M. Cheng, Nitrogen-Doped Carbon Monolith for Alkaline Supercapacitors and Understanding Nitrogen-Induced Redox Transitions, Chemistry – A European Journal, 18 (2012) 5345-5351.[50] W. Kim, M.Y. Kang, J.B. Joo, N.D. Kim, I.K.

Song, P. Kim, J.R. Yoon, J. Yi, Preparation of ordered mesoporous carbon nanopipes with controlled nitrogen species for application in electrical double-layer capacitors, J. Power Sources, 195 (2010) 2125-2129.

[51] J.W. Lee, J.M. Ko, J.-D. Kim, Hydrothermal preparation of nitrogen-doped graphene sheets via hexamethylenetetramine for application as supercapacitor electrodes, Electrochim. Acta, 85 (2012) 459-466.

[52] G. Lota, K. Lota, E. Frackowiak, Nanotubes based composites rich in nitrogen for supercapacitor application, Electrochem. Commun., 9 (2007) 1828-1832.

[53] B. Xu, S. Yue, N. Qiao, M. Chu, G. Wei, Easy preparation of nitrogen-doped porous carbon nanospheres and their application in supercapacitors, Mater Lett, 131 (2014) 49-52.

[54] E. Raymundo-Piñero, M. Cadek, F. Béguin, Tuning Carbon Materials for Supercapacitors by Direct Pyrolysis of Seaweeds, Adv. Funct. Mater., 19 (2009) 1032-1039.

[55] Y. Korenblit, M. Rose, E. Kockrick, L. Borchardt, A. Kvit, S. Kaskel, G. Yushin, High-Rate Electrochemical Capacitors Based on Ordered Mesoporous Silicon Carbide-Derived Carbon, ACS Nano, 4 (2010) 1337-1344.

[56] L. Qie, W. Chen, H. Xu, X. Xiong, Y. Jiang, F. Zou, X. Hu, Y. Xin, Z. Zhang, Y. Huang, Synthesis of functionalized 3D hierarchical porous carbon for high-performance supercapacitors, Energy Environ. Sci., 6 (2013) 2497-2504.

[57] Y. Li, Z. Li, P.K. Shen, Simultaneous Formation of Ultrahigh Surface Area and Three-Dimensional Hierarchical Porous Graphene-Like Networks for Fast and Highly Stable Supercapacitors, Adv. Mater., 25 (2013) 2474-2480.

[58] Y. Yuanyuan, L. Ruiyi, L. Zaijun, L. Junkang, G. Zhiguo, W. Guangli, A facile self-template strategy to fabricate three-dimensional nitrogen-doped hierarchical porous carbon/graphene for conductive agent-free supercapacitors with excellent electrochemical performance, Electrochim. Acta, 125 (2014) 330-337.